Optical Properties and Ultrafast Near-Infrared Localized Surface Plasmon Dynamics in Naturally p-Type Digenite Films

ADVANCED OPTICAL MATERIALS
www.advopticalmat.de

Optical Properties and Ultrafast Near-Infrared Localized Surface Plasmon Dynamics in Naturally p-Type Digenite Films

Andrea Villa, Madina Telkhozhayeva, Fabio Marangi, Eti Teblum, Aaron M. Ross, Mirko Prato, Luca Andena, Roberto Frassine, Francesco Scotognella, and Gilbert Daniel Nessim*

Copper chalcogenides are materials characterized by intrinsic doping properties, allowing them to display high carrier concentrations due to their defect-heavy structures, independent of the preparation method. Such high doping enables these materials to display plasmonic resonances, tunable by varying their stoichiometry. Here, plasmonic dynamics is studied in drop-cast Cu_9S_5 (digenite) nanocrystals (NCs) film using ultrafast pump–probe spectroscopy. The NCs are synthesized by thermal annealing of copper foil using chemical vapor deposition (CVD), followed by sonication and drop-casting of the isolated few-layered flakes on different substrates. The samples display a broad localized surface plasmon resonance (LSPR) in the near-infrared (NIR), peaking at 2100 nm. The free carrier response is further confirmed by fitting the linear absorption with a Drude–Lorentz effective medium approximation model. The high temporal resolution allows to measure the relaxation dynamics of the photo-excited holes, which are dominated by a fast decay ($\tau_1 = 360 \pm 20$ fs) and correspond to hole–phonon scattering processes, followed by a long-lived ($\tau_2 > 1$ ns) signal associated with phonon–phonon scattering relaxation. These results confirm the possibility of fabricating Cu_9S_5 films retaining the plasmonic properties of individual NCs, anticipating integrating these films into heterojunctions with suitable hole acceptor materials to build hot-hole-transfer-based optoelectronic devices.

1. Introduction

Heavily doped semiconductors have been gaining increasing attention in the last decades.[1,2] In the 1960–70s, reports were published on copper chalcogenide films and single crystals characterized by remarkable intrinsic doping, also called "self-doping."[3,4] In particular, Abdullaev et al. studied the temperature dependence of several properties in Cu_2Se single crystals, including conductivity, thermoelectromotive force and Hall constant, which allowed them to estimate the concentration and mobility of the carriers in the crystals.[3] Further studies on copper chalcogenides by Gorbachev et al. led to the determination of the effective mass of holes (m_h) in Cu_2Se and Cu_2Te as a function of both carrier concentration and temperature, associating the dependence of m_h on carrier density to the non-parabolic character of the valence band of the materials.[4] Both these materials are intrinsically degenerate p-type semiconductors, independently of the preparation

A. Villa, F. Marangi, A. M. Ross, F. Scotognella
Department of Physics
Politecnico di Milano
Milan 20133, Italy
E-mail: francesco.scotognella@polimi.it

M. Telkhozhayeva, G. D. Nessim
Department of Chemistry
Bar-Ilan University
Ramat Gan 5290002, Israel

The ORCID identification number(s) for the author(s) of this article can be found under https://doi.org/10.1002/adom.202201488.

DOI: 10.1002/adom.202201488

F. Marangi, F. Scotognella
Center for Nano Science and Technology@PoliMi
Istituto Italiano di Tecnologia (IIT)
Milan 20133, Italy

E. Teblum, G. D. Nessim
Bar-Ilan Institute of Nanotechnology & Advanced Materials (BINA)
Ramat Gan 5290002, Israel

M. Prato
Materials Characterization Facility
Istituto Italiano di Tecnologia (IIT)
Genova 16163, Italy

L. Andena, R. Frassine
Department of Chemistry, Materials and Chemical Engineering "G. Natta"
Politecnico di Milano
Milan 20133, Italy

method, and characterized by carrier concentrations between 10^{19} and 10^{22} cm^{-3}, as their Fermi levels lie inside the valence band.[4] This characteristic of copper chalcogenides makes them very interesting for practical applications, because by acting on their stoichiometry it is possible to choose the desired balance between carrier density and m_h, tailoring the materials characteristics to better suit the desired application. Specifically, it has been observed that m_h increases progressively with the density of carriers, due to the material displaying more Cu vacancies and related defects which hinder the overall mobility of the holes.[5] It is therefore possible to either have low carrier density with very high mobility, which is preferable for applications such as high-speed electronics,[6] or high carrier densities with low mobility, which leads to strong free carrier absorption and localization effects which can be of interest for plasmonic applications.[7]

Among copper chalcogenides, copper sulfide has been extensively studied.[8] Important characteristics of copper sulfide are non-toxicity, the abundance of copper and sulfur elements, and low fabrication costs.[9,10] Depending on the synthesis method, the stoichiometric factor (x) in $Cu_{2-x}S$ varies from the most Cu-rich Cu_2S (chalcocite) to the most Cu-poor CuS (covellite), including many non-stoichiometric phases in between, such as $Cu_{1.97}S$ (djurleite), Cu_9S_5 (digenite), Cu_7S_4 (anilite), etc.[11] Their p-type electronic character is associated with lattice cation vacancy formation. Doping by copper vacancy formation happens because of the low chemical potential and high mobility of copper ions.[12] An increase in Cu deficiency in non-stoichiometric copper sulfides leads to a partial filling of sulfur 3p orbitals, which leads to a higher concentration of holes, resulting in a progressive blue-shift and increase in the intensity of the localized surface plasmon resonance (LSPR).[13,14] In contrast, the full stoichiometric Cu_2S does not exhibit any LSPR absorbance due to the absence of any free holes, and its valence band is completely filled. This indicates that the LSPRs of $Cu_{2-x}S$ are highly dependent on their stoichiometries and hence crystal structures, as was first demonstrated by Zhao et al., who investigated the optical and structural properties of CuS, $Cu_{1.8}S$ and $Cu_{1.97}S$ nanocrystals (NCs).[12] Similar properties were also reported for other copper chalcogenides such as $Cu_{2-x}Se$ by Dorfs et al.,[13] who investigated the possibility of reversibly tuning the position of the LSPR. This can be done by acting on the stoichiometry of the NCs, increasing or reducing the number of copper vacancies through oxidation or addition of Cu(I) complexes, respectively. Other key parameters to tune the LSPR are the dimensions and morphology of the NCs, as demonstrated in $Cu_{2-x}S$ quantum dots,[15] nanosheets,[16] nanodisks,[17] and nanoplates.[18] Although synthesis and optical properties of copper sulfides have been widely explored, especially in the case of stoichiometric CuS NCs,[16,19,20] there is limited literature on digenite NCs films.

Digenite (Cu_9S_5, $x = 0.2$) is distinguished as a steady phase, which exists in two modifications: low-digenite (below 364 K) and high-digenite (above 364 K).[21] Crystals of digenite are found to be cubic or hexagonal and are based on the fcc sublattice of S. This structure is similar to the one of cubic chalcocite (Cu_2S), except that only 9/10 of the Cu sites are occupied.[22] First studies on the optical properties of copper-based sulfides were performed by B. J. Mulder, who determined the absorption and reflection spectra between 400 and 1200 nm of Cu_9S_5 films obtained through controlled oxidation of chalcocite thin single crystals.[23] Further studies by Rajkanan determined the optical constants in the range 1.1–2.7 eV of copper sulfide with different stoichiometries, showing that the imaginary part of the refractive index (i.e., k) of $Cu_{1.77}S$ increases toward lower energies.[24] Grozdanov and Najdoski later confirmed a decrease in transmission at wavelengths longer than 1 μm, ascribing such absorption feature to interband excitation of free carriers.[25] In all the studies mentioned above, the films under investigation were obtained through chemical deposition or conversion of different phases of copper sulfide and not directly from bulk digenite. Further investigations of the ultrafast optical properties of stable dispersions of several copper chalcogenides, including $Cu_{2-x}S$ NCs, were performed by Kriegel et al., who demonstrated the possibility of reversibly controlling and tuning the LSPR of the NCs by acting on their copper deficiency.[26] Additional studies on the ultrafast optical response of colloidal NCs of $Cu_{2-x}S$ and $Cu_{2-x}Se$ were performed by Xie et al. and Scotognella et al., who investigated the size-dependence of the LSPR,[27] and the fluence-dependence of carrier dynamics following resonant excitation of the plasmonic mode, respectively.[28] Although several studies on the ultrafast carrier dynamics of colloidal dispersions of NCs were reported, the possibility of using these NCs to form thin films with strong plasmonic properties has not been investigated yet.

In this work, we report the fabrication and optical characterization of drop-cast digenite NCs films, which display near-infrared (NIR) plasmonic absorption at 2100 nm. The NCs were obtained by powdering bulk Cu_9S_5 grown by reactive thermal annealing of copper foil using chemical vapor deposition (CVD), then dispersed in different solvents to identify the optimum conditions for a stable solution. The solution was later drop-cast onto various substrates such as glass and ITO/glass to form thin films, which were subsequently characterized by different techniques. The transient optical response of the film following photoexcitation of the NCs' NIR plasmonic resonance was investigated in the visible and NIR spectral ranges using ultrafast pump–probe spectroscopy (**Figure 1**). Even in the aggregated state, the films display the typical response of heavily doped semiconductor NCs, with a faster decay ($\tau_1 = 360 \pm 20$ fs) associated with hole–phonon scattering processes, followed by a slower one ($\tau_2 > 1$ ns), which can be explained by phonon–phonon relaxation. This work demonstrates the possibility of exploiting reactive thermal annealing, which allows increased and faster bulk material production compared to wet chemistry synthesis, and drop-casting, an easy and fast technique, to form Cu_9S_5 films displaying absorption in the NIR. We anticipate integrating the Cu_9S_5 films into hot-hole-harvesting optoelectronic devices showing NIR absorption by coupling with suitable hole acceptor materials.

2. Results and Discussion

SEM images were acquired to visualize the morphology of both bulk and subsequently drop-cast Cu_9S_5 flakes. Due to the well-defined stacked-layered structure of the bulk Cu_9S_5 (**Figure 2**a), it could be readily exfoliated into thin 2D flakes

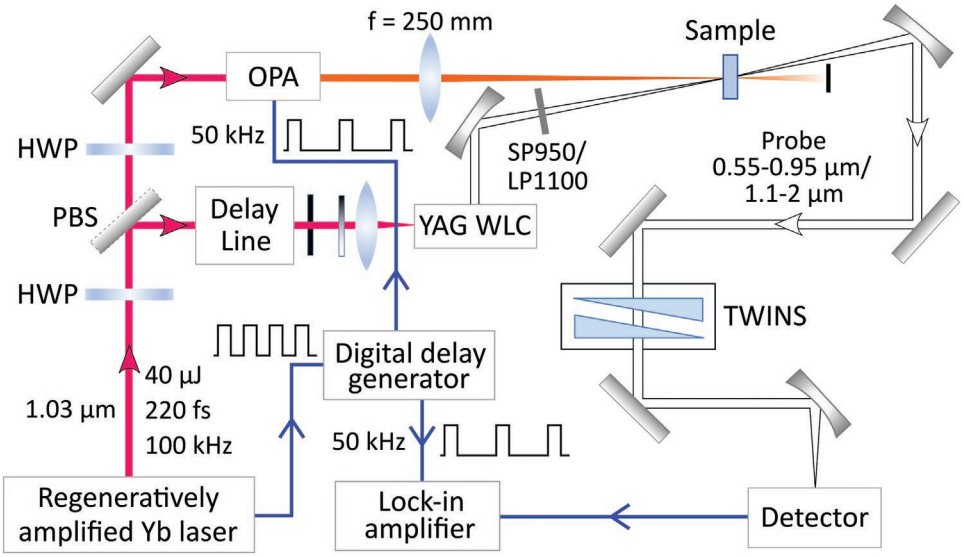

Figure 1. Scheme of the setup used for the ultrafast pump–probe measurements.

having a dimension of a few hundred of nm with clear and sharp edges as shown in Figure 2b. Moreover, a sheet-like substructure could be evidenced in those of greater dimensions, as reported previously for the bulk.[10] Although SEM does not allow to determine the thickness of the flakes; the observed structure suggests that, with the use of the established liquid exfoliation technique, a greater number of few-atom-thick flakes could be obtained. To confirm this, we performed AFM analysis to measure the thickness of the flakes drop-cast on Si/SiO_2—300 nm substrate. Figure S1 (Supporting Information) shows that thin Cu_9S_5 flakes are roughly 4 nm thick. The observed height is slightly larger than the typical thickness of exfoliated transition metal chalcogenides (TMCs) layers (1–2 nm). Such thickness deviation could potentially be attributed to the absorbed solvent molecules.[29] Thus, we successfully isolated the bulk digenite down to few-layered flakes.

Figure 3a reports the results of the UPS measurements performed on the films. The left plot shows the intensity of the secondary electron emission upon He I excitation as a function of the kinetic energy of the photoelectrons. The photoemission onset is directly correlated with the work function of a material, which can be identified either directly with the signal onset, or with the middle point of the sharpest slope close to the signal onset, in order to account for instrumental and thermal broadening effects, as reported in a previous work by Park et al.[30] The retrieved values for the work function for digenite film using the two criteria were respectively 4.0 ± 0.1 eV, which is lower than what was reported in previous literature, and 4.5 ± 0.1 eV, which is in agreement with the reported calculated work function of Cu_9S_5.[31] The right plot reports the intensity of the photoelectron emission as a function of the binding energy. From this plot, the position of the VBM can be obtained by extracting the low binding energy onset of the photoelectron emission (magnified in the inset), assuming the Fermi level is at the zero of the binding energy scale. For the samples under investigation, the onset of the emission is found to be very close to zero, confirming that the Fermi level of the films is close to the VBM, in agreement with the p-type character of the material.

The linear absorption spectrum of the films in the region between 500 and 2500 nm is reported in Figure 3b. Scattering contributions from the samples, which cannot be considered

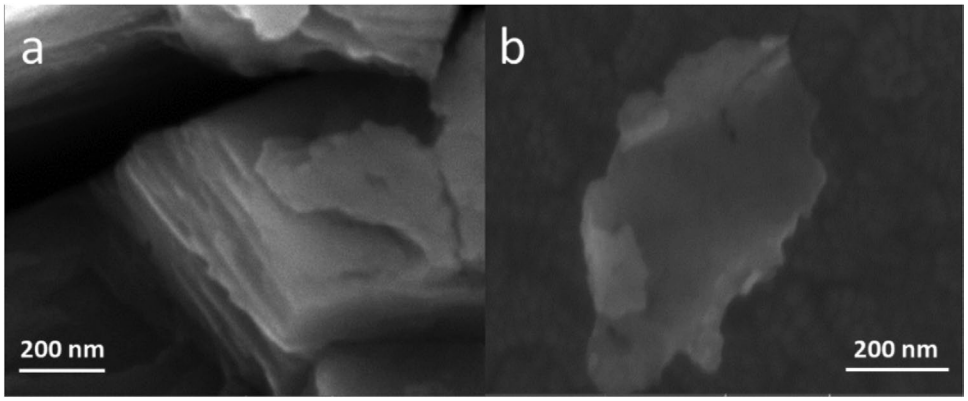

Figure 2. Scanning electron microscopy (SEM) images of a) bulk and b) drop-cast Cu_9S_5 flakes.

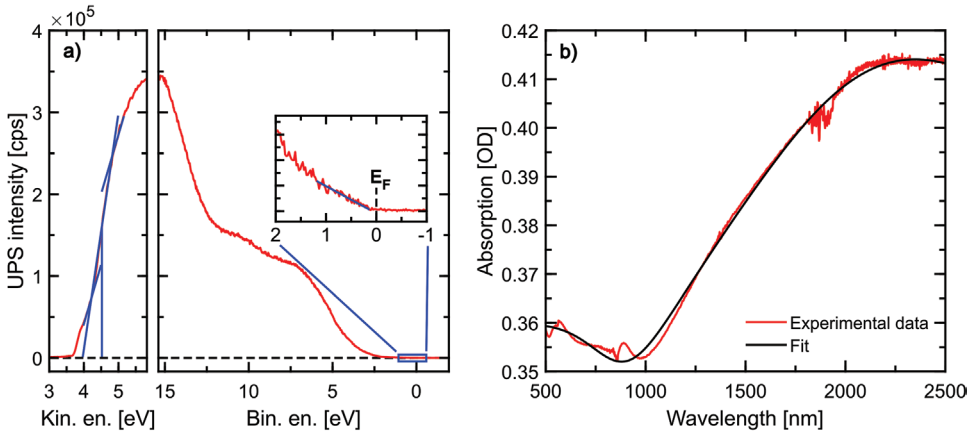

Figure 3. Results of ultraviolet photoelectron spectroscopy (UPS) measurements of bulk Cu_9S_5 and linear absorption of a drop-cast Cu_9S_5 NCs film. a) Results of the UPS measurements, where the intensity of the photoelectron emission is reported as a function of both the kinetic and binding energy of the photoelectrons. Magnifications of the low and high kinetic energy tails are provided along with blue vertical lines to highlight better the values of the work function and valence band maximum of the material, respectively. b) Results of the linear absorption measurements, where the experimental data are reported in red, while the black solid curve corresponds to a fit exploiting the Drude–Lorentz model along with the effective medium approximation.

negligible given the highly inhomogeneous nature of the NCs films, were taken into account using an integrating sphere. A remarkable absorption band is observed in the NIR region beyond 1000 nm, with a noticeable peak at 2100 nm. However, due to experimental limitations, it was not possible to observe the low energy tail of the peak. Given the sub-stoichiometric nature of Cu_9S_5, which displays the characteristics of a strongly degenerate p-type semiconductor, as confirmed by the UPS analyses described in the previous paragraph, the observed peak can be ascribed to plasmonic absorption by the free carriers of the material. Therefore, the absorption of the films of deposited NCs is similar to what was reported in previous works for stable solutions of $Cu_{2-x}S$ quantum dots[15] and NCs with reversibly tunable LSPR,[26] which were, however, fabricated through wet chemistry synthesis.

The experimental data were fitted using the Drude–Lorentz model along with the effective medium approximation:[32] the drop-cast film was assumed as composed of Cu_9S_5 NCs and air voids, with starting parameters retrieved from existing literature.[14] The retrieved carrier density was $N = 4.5 \times 10^{21} cm^{-3}$, the hole effective mass $m_h^* = 0.95\, m_e$ (where m_e is the free electron mass), the high frequency dielectric function $\varepsilon_\infty = 2.0$, and the band linewidth $\Gamma = 0.56$ eV, from which the plasmon dephasing time could be estimated at around $T_2 = 2.35$ fs. The thickness of the flakes was found to be around 5 nm, while the porosity, intended as the fraction of volume occupied by air in the film, was estimated to be 0.12. To account for any residual scattering from the nanocrystalline film, a term with E^4 dependence was added to the fitted curve, E being the energy.

Results of the ultrafast pump–probe measurements performed on the drop-cast Cu_9S_5 NCs film for the infrared (IR) and visible probe configurations are presented in **Figures 4** and **5**, respectively, with the retrieved differential transmission maps for pump–probe delays below 3 ps as displayed in Figures 4a and 5a. Since the optical bandgap of Cu_9S_5 is greater than 1.1 eV while excitation is performed with pulses centered at about 1800 nm, which corresponds to a photon energy of 0.69 eV, the retrieved signal can be ascribed to intraband excitation of the free carriers of the material. The measured signal can be interpreted by exploiting the two-temperature model for the ultrafast thermal response of photoexcited plasmonic materials.[28,33] Immediately following excitation, the plasmon oscillations rapidly dephase through Landau damping in a few femtoseconds, generating a non-thermal distribution of hot holes in the valence band of Cu_9S_5. Said hot carrier distribution then proceeds to cool down through hole–hole scattering processes on a timescale below 100 fs to a Fermi–Dirac distribution characterized by a high-temperature T_h for the hole gas. This hot distribution later further relaxes through hole–phonon scattering, cooling down by transferring energy to the material's lattice, heating it up on a timescale of a few picoseconds. The lattice then releases heat to the environment, completely relaxing on timescales between hundreds of picoseconds and few nanoseconds. While the duration of the pump of 50 fs does not allow to resolve the plasmon dephasing and hole–hole scattering processes taking place immediately after photoexcitation,[14] the dynamics of the slower hole–phonon and phonon–phonon scattering relaxation can be fully resolved (Figures 4b,c and 5b,c).

In general, by pumping the plasmonic resonance and probing in the NIR, the sample displays bleaching across the entire spectrum, which can be explained as a reduction in the number of holes available for promotion to higher energy states after photoexcitation and a consequent redshift of the plasmonic resonance (Figure 4). Instead, by pumping in the IR and probing in the visible, a negative differential transmission signal is observed in the entire 530–730 nm region (Figure 5). This signal can be explained by an increased possibility for electrons in the valence band to be promoted to the conduction band after IR photoexcitation, as new transition pathways are made available for electrons initially promoted to the top of the valence band by the IR pump pulses. The signals in visible and IR display similar dynamics and timescales, as it can be estimated from the results of the global analysis fits performed on the retrieved pump-probe maps (see "Global Analysis" Section, Supporting Information), confirming that they both originate

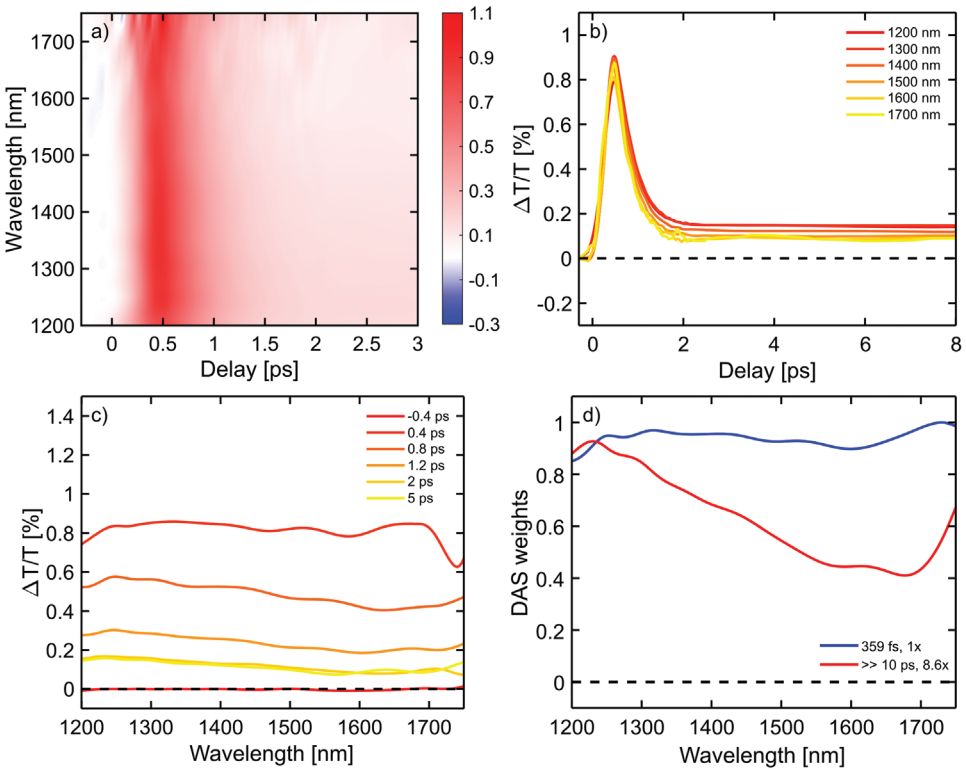

Figure 4. Results of the ultrafast differential transmission measurements performed on the drop-cast Cu_9S_5 NCs film probing between 1200 and 1800 nm. a) Pump–probe map for delays below 3 ps. b) Dynamics at different wavelengths for delays up to 10 ps. c) Differential transmission spectra at increasing pump–probe delays. d) Results of the global analysis fit performed using a bi-exponential decay.

from the excitation of the plasmonic resonance of the free carriers of the material. Given the available temporal resolution guaranteed by the pump-pulses used in the experiment, a bi-exponential fit was performed to retrieve the hole–phonon scattering rate while also considering the long-lived component associated with phonon–phonon scattering. The fastest process is characterized by a time constant $\tau_1 = 302 \pm 20$ fs in the visible and $\tau_1 = 359 \pm 20$ fs in the IR, so that the hole–phonon scattering is completely exhausted within the first 1.5–1.75 ps after photoexcitation, while for the long-lived component, a lifetime $\tau_2 \gg 10$ ps was retrieved. Since this lifetime is much longer than the maximum pump–probe delay used for the measurement, it is safe to assume that this second component is associated with phonon–phonon scattering, which is usually characterized by much longer lifetimes. Single wavelength measurements (Figure S2, Supporting Information) performed at 1200 and 1300 nm (Figure S3, Supporting Information) with the same excitation pulses but a much longer delay range showed that the long-lived component is not completely decayed even after 1 ns. For additional information see the "Single Wavelength Measurements" Section (Supporting Information). Further measurements were performed to try to investigate the plasmon dynamics close to the resonance peak, using a 2000 nm probe (Figure S5, Supporting Information), but the excessive noise made the measurement not completely reliable. While the signal at short times looks very similar to what is observed at other IR wavelengths, at longer times there might be a reversal of the sign, with the signal becoming negative. Nonetheless, further experiments should be performed with a stronger and more red-shifted IR probe to properly confirm the nature of the signal at longer times. The results of the measurement are reported in the "Plasmonic Peak Dynamics" Section (Supporting Information).

3. Conclusion

We investigated the optical properties and ultrafast carrier dynamics in drop-cast Cu_9S_5 NCs film, retrieving the lifetime of the photoexcited carriers following resonant excitation of the plasmonic resonance of the material. UPS characterization confirmed the strongly degenerate p-type character of the material, which along with its layered crystalline structure, makes this copper chalcogenide promising for integration into thin p–n heterojunctions with TMCs and other similar 2D materials.[10,34] We demonstrated that drop-casting of a stable dispersion of the ground bulk material in DMF is a viable solution for fabricating thin films consisting of a few layers of Cu_9S_5, which allows avoiding more complex fabrication techniques involving chemical deposition and processing or wet chemistry synthesis. The fabricated films displayed a broad IR plasmonic resonance located at around 2000 nm, arising from the excess of free holes of Cu_9S_5 induced by its stoichiometry. The ultrafast optical properties of the films after intraband excitation of their free carriers were inspected through pump–probe spectroscopy, and the response was interpreted according to the

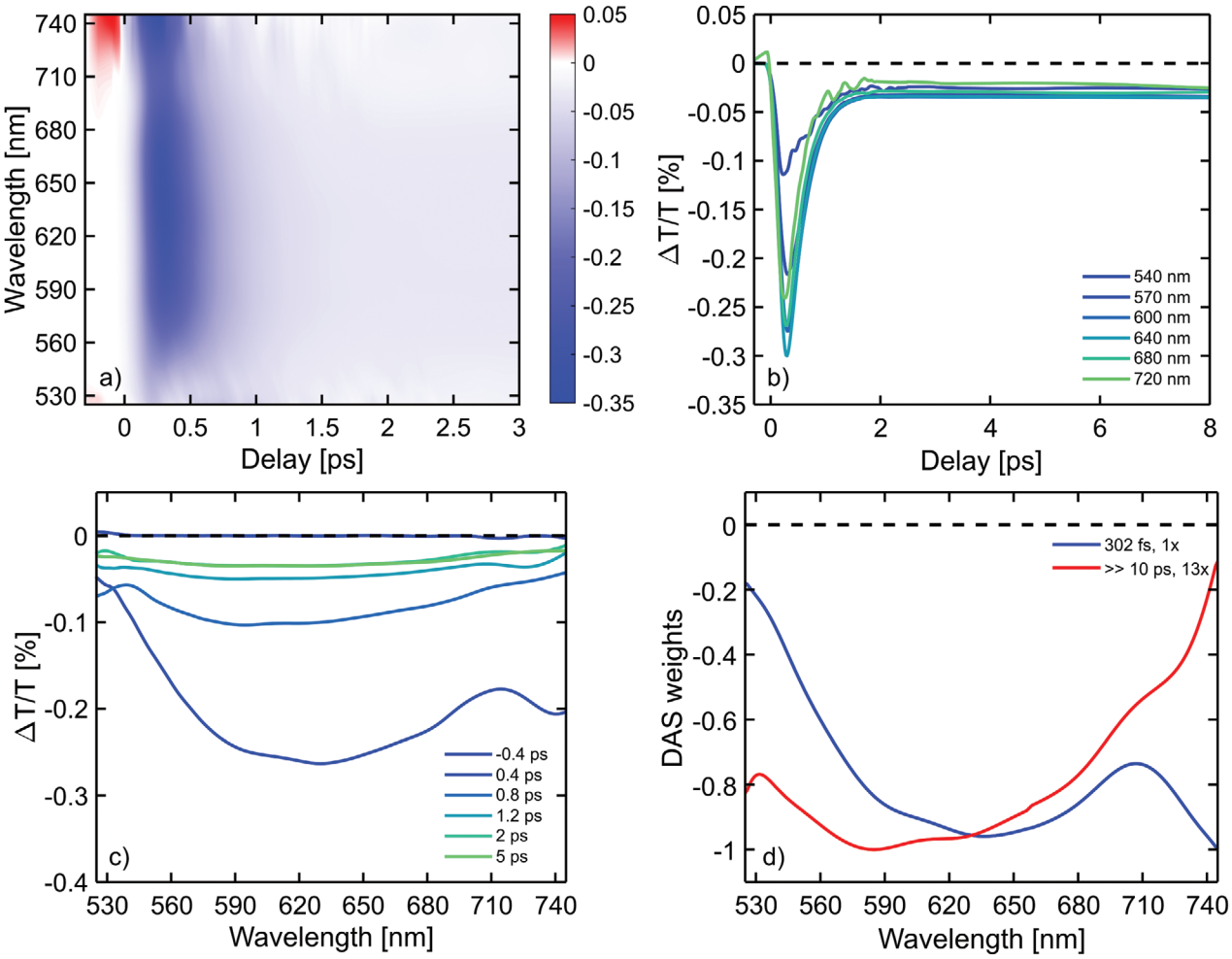

Figure 5. Results of the ultrafast differential transmission measurements performed on the drop-cast Cu_9S_5 NCs film probing between 520 and 750 nm. a) Pump–probe map for delays below 3 ps. b) Dynamics at different wavelengths for delays up to 8 ps. c) Differential transmission spectra at increasing pump–probe delays. d) Results of the global analysis fit performed using a bi-exponential decay.

two-temperature model. The lifetimes τ_1 and τ_2 for the hole–phonon and phonon–phonon scattering processes happening after the dephasing of the LSPR were retrieved, estimating values of $\tau_1 = 359 \pm 20$ fs and $\tau_1 = 302 \pm 20$ fs for IR and visible measurements, respectively, while τ_2 was found to be much larger than the longest scanned pump–probe delay. Determining these values, which are consistent with previous literature on colloidal NCs of copper chalcogenides,[26] constitutes the first step in understanding the dynamics of free carriers in thin films of Cu_9S_5 before their integration in optoelectronic devices.

4. Experimental Section

Synthesis of Bulk Cu_9S_5: All reagents used in the synthesis were of analytical grade without further purification. Bulk digenite was synthesized using atmospheric pressure CVD composed of two furnaces (Lindberg Blue). The furnaces were equipped with a quartz tube, while the temperatures were monitored using built-in furnace thermocouples. Synthesis of bulk Cu_9S_5 was reported in a previous work.[10] Typically, the temperatures were set at 450 °C for the furnace with elemental sulfur and 650 °C for the furnace with copper foil. The growth was performed for 15 min in an inert atmosphere (Ar, 99.9999%, Gas Technologies). The S source (sulfur powder, Alfa Aesar, 99.5%) was positioned upstream of the gas flow in the first furnace, and a 1 cm × 1 cm piece of copper foil (Alfa Aesar, 99.9%) was placed downstream in the second furnace. Before the experiment, the quartz tube was purged with Ar gas until the furnace reached equilibrium at given temperatures in two zones. At the end of the reaction process, the "fast heat" technique was used.[35]

Sample Preparation: The fabrication of the samples for further characterizations was carried out starting from the bulk material. A small amount of material was powdered to get finer grain sizes using a mortar and then dispersed in various solvents. Stable dispersions of copper sulfide nanostructures of different shapes and dimensions were reported in water, ethylene glycol, dimethylformamide (DMF), and dimethyl sulfoxide (DMSO).[36–40] Similarly, copper sulfide powder was dispersed in these solvents at different concentrations. The most stable dispersion, which could then be drop-cast, was the one in DMF, with a concentration of 7.5 mg L^{-1}. Samples for linear absorption and pump–probe measurements were obtained by drop-casting the dispersion on pre-heated glass slides, while those for other measurements were drop-cast on ITO/glass and Si/SiO_2-300 nm substrates.

Scanning Electron Microscopy (SEM): The morphology of the samples was investigated using SEM. The images were acquired by using a SEM Tescan Mira 3 instrument.

Atomic Force Microscope (AFM): AFM measurements were carried out by a Bio FastScan scanning probe microscope (Bruker AXS). All images were obtained by using PeakForce QNM (PeakForce Quantitative Nanomechanical Mapping) mode with a FastScan-C (Bruker) silicon probe (spring constant of 0.45 N m^{-1}). The measurements were performed under environmental conditions in the acoustic hood to minimize vibrational noise. The images were captured in the retrace direction with a scan rate of 1.6 Hz. The resolution of the images was 512 samples per line. For image processing and thickness analysis, Nanoscope Analysis software was used. The "flatting" and "planefit" functions were applied to each image.

Ultraviolet Photoelectron Spectroscopy (UPS): UPS analyses were carried out using a Kratos Axis Ultra^{DLD} spectrometer, using a He I (21.22 eV) discharge lamp on an area of 55 µm in diameter, at pass energy of 5 eV and with a dwell time of 100 ms. The work function was measured from the threshold energy for the emission of secondary electrons during He I excitation. A negative bias of 9.0 V was applied to the sample to determine the low-kinetic-energy cutoff precisely. Then, the position of the valence band maximum (VBM) versus the vacuum level was estimated by measuring its distance from the Fermi level.

Linear Absorption: UV–vis–NIR absorption spectra were acquired with a Perkin Elmer Lambda 1050 WB spectrophotometer. The instrument was equipped with deuterium (280–320 nm) and tungsten (320–3300 nm) lamps. The signal was recorded by three detectors working in different spectral regions (photomultiplier [180, 860] nm, InGaAs [860, 1300] nm, and PbS [1300, 3300] nm), with the possibility of taking into account scattering contributions by using an integrating sphere.

Ultrafast Transient Absorption (TA): TA pump–probe measurements were performed on the samples to investigate the plasmonic dynamics of the drop-cast Cu_9S_5 film by retrieving the differential transmission $\Delta T/T$. The scheme of the setup used for the measurements is shown in Figure 1. The measurements were carried out by exciting the samples with pulses generated by a two-stage optical parametric amplifier (OPA) supplied by a regeneratively amplified Yb laser (Pharos, Light Conversion), which provides 50 µJ, 220-fs-long pulses at 1030 nm and 100 kHz repetition rate.[41] For the generation of pump pulses, the OPA was tuned to provide 50-fs-long pulses centered at around 1800 nm in the region of the plasmonic resonance of digenite. The repetition rate of said pulses was set to 50 kHz using a Pockels cell (Eksma Optics), inserted in the OPA before the generation of the seed, and driven by a digital delay generator (Model 525, Berkeley Nucleonics). The probe pulses were achieved at 100 kHz repetition rate, exploiting white light generation in two different YAG crystals pumped by a fraction of the energy of the pulses coming from the laser. Two different spectral regions were inspected in the infrared between 1200 and 1750 nm using white light obtained from a 1-cm-long YAG and visible range between 530 and 730 nm exploiting pulses generated in a 4-mm-long YAG.[42] The detection system consisted of an interferometric spectrometer based on a birefringent delay line (GEMINI, Nireos),[43–46] followed by two different detectors, depending on the spectral region of interest. Measurements in the infrared were performed using an amplified thermoelectrically cooled InAsSb detector (PDA10PT, Thorlabs) sensitive between 1000 and 5800 nm, while those in the visible exploited a Si biased photodiode (DET100A2, Thorlabs) connected to a transimpedance amplifier. The signals from the detector were subsequently demodulated by a lock-in amplifier (Zürich Instruments MFLI) triggered by the digital delay generator to retrieve the T_{off} and ΔT signals. This arrangement provides a high signal-to-noise ratio by fully exploiting the high repetition rate of the system. Detailed information on the data processing of collected pump–probe data is described in the "Broadband Pump–Probe Data Processing" Section (Supporting Information) (Figures S5–S10, Supporting Information).

Supporting Information

Supporting Information is available from the Wiley Online Library or from the author.

Acknowledgements

A.V., M.T., and F.M. contributed equally to this work. This work was supported and funded by the European Research Council (ERC) under the European Union's Horizon 2020 research and innovation program (Grant Agreement No. 816313).

Conflict of Interest

The authors declare no conflict of interest.

Data Availability Statement

The data that support the findings of this study are available from the corresponding author upon reasonable request.

Keywords

copper chalcogenides, digenite nanocrystals film, localized surface plasmon resonance, ultrafast spectroscopy

Received: June 27, 2022
Revised: October 3, 2022
Published online:

[1] A. Agrawal, R. W. Johns, D. J. Milliron, *Annu. Rev. Mater. Res.* **2017**, *47*, 1.
[2] F. Marangi, M. Lombardo, A. Villa, F. Scotognella, *J. Ocul. Pharmacol. Ther.* **2021**, *11*, 100083.
[3] G. B. Abdullaev, Z. A. Aliyarova, G. A. Asadov, *Phys. Status Solidi* **1967**, *21*, 461.
[4] V. V. Gorbachev, I. M. Putilin, *Phys. Status Solidi* **1973**, *16*, 553.
[5] Z. H. Li, K. O. Egbo, X. H. Lv, Y. Wang, K. M. Yu, C. P. Liu, *Appl. Surf. Sci.* **2022**, *572*, 151530.
[6] B. A. D. Williamson, J. Buckeridge, J. Brown, S. Ansbro, R. G. Palgrave, D. O. Scanlon, *Chem. Mater.* **2017**, *29*, 2402.
[7] I. Kriegel, J. Rodríguez-Fernández, A. Wisnet, H. Zhang, C. Waurisch, A. Eychmüller, A. Dubavik, A. O. Govorov, J. Feldmann, *ACS Nano* **2013**, *7*, 4367.
[8] Y. Liu, M. Liu, M. T. Swihart, *J. Phys. Chem. C* **2017**, *121*, 13435.
[9] Y. He, T. Day, T. Zhang, H. Liu, X. Shi, L. Chen, G. J. Snyder, *Adv. Mater.* **2014**, *26*, 3974.
[10] A. Itzhak, E. Teblum, O. Girshevitz, S. Okashy, Y. Turkulets, L. Burlaka, G. Cohen-Taguri, E. Shawat Avraham, M. Noked, I. Shalish, G. D. Nessim, *Chem. Mater.* **2018**, *30*, 2379.
[11] D. J. Chakrabarti, D. E. Laughlin, *Bull. Alloy Phase Diagrams* **1983**, *4*, 254.
[12] Y. Zhao, H. Pan, Y. Lou, X. Qiu, J. Zhu, C. Burda, *J. Am. Chem. Soc.* **2009**, *131*, 4253.
[13] D. Dorfs, T. Härtling, K. Miszta, N. C. Bigall, M. R. Kim, A. Genovese, A. Falqui, M. Povia, L. Manna, *J. Am. Chem. Soc.* **2011**, *133*, 11175.
[14] I. Kriegel, F. Scotognella, L. Manna, *Phys. Rep.* **2017**, *674*, 1.
[15] J. M. Luther, P. K. Jain, T. Ewers, A. P. Alivisatos, *Nat. Mater.* **2011**, *10*, 361.
[16] R. Lesyuk, E. Klein, I. Yaremchuk, C. Klinke, *Nanoscale* **2018**, *10*, 20640.
[17] S.-W. Hsu, W. Bryks, A. R. Tao, *Chem. Mater.* **2012**, *24*, 3765.

[18] X. Wang, Y. Ke, H. Pan, K. Ma, Q. Xiao, D. Yin, G. Wu, M. T. Swihart, *ACS Catal.* **2015**, *5*, 2534.
[19] M. Huang, X. Wang, G. Xing, C. Meng, Y. Li, X. Li, L. Fan, Y. Wan, S. Yang, *J. Phys. Chem. Lett.* **2021**, *12*, 7988.
[20] R. M. Córdova-Castro, M. Casavola, M. van Schilfgaarde, A. V. Krasavin, M. A. Green, D. Richards, A. V. Zayats, *ACS Nano* **2019**, *13*, 6550.
[21] G. Will, E. Hinze, A. R. M. Abdelrahman, *Eur. J. Mineral.* **2002**, *14*, 591.
[22] P. Lukashev, W. R. L. Lambrecht, T. Kotani, M. Van Schilfgaarde, *Phys. Rev. B: Condens. Matter Mater. Phys.* **2007**, *76*, 195202.
[23] B. J. Mulder, *Phys. Status Solidi* **1972**, *13*, 79.
[24] K. Rajkanan, Preparation and Characterization of Thin Copper Sulfide Films for Their Application in Solar Cells, Thesis, McMaster University, Hamilton, Ontario **1978**.
[25] I. Grozdanov, M. Najdoski, *J. Solid State Chem.* **1995**, *114*, 469.
[26] I. Kriegel, C. Jiang, J. Rodríguez-Fernández, R. D. Schaller, D. V. Talapin, E. Da Como, J. Feldmann, *J. Am. Chem. Soc.* **2012**, *134*, 1583.
[27] Y. Xie, L. Carbone, C. Nobile, V. Grillo, S. D'Agostino, F. Della Sala, C. Giannini, D. Altamura, C. Oelsner, C. Kryschi, P. D. Cozzoli, *ACS Nano* **2013**, *7*, 7352.
[28] F. Scotognella, G. D. Valle, A. R. Srimath Kandada, D. Dorfs, M. Zavelani-Rossi, M. Conforti, K. Miszta, A. Comin, K. Korobchevskaya, G. Lanzani, L. Manna, F. Tassone, *Nano Lett.* **2011**, *11*, 4711.
[29] X. Song, G. Cheng, D. Weber, F. Pielnhofer, S. Lei, S. Klemenz, Y.-W. Yeh, K. A. Filsinger, C. B. Arnold, N. Yao, L. M. Schoop, *J. Am. Chem. Soc.* **2019**, *141*, 15634.
[30] Y. Park, V. Choong, Y. Gao, B. R. Hsieh, C. W. Tang, *Appl. Phys. Lett.* **1996**, *68*, 2699.
[31] Z. Peng, S. Li, M. Weng, M. Zhang, C. Xin, Z. Du, J. Zheng, F. Pan, *J. Phys. Chem. C* **2017**, *121*, 23317.
[32] Y. Battie, A. E. Naciri, W. Chamorro, D. Horwat, *J. Phys. Chem. C* **2014**, *118*, 4899.
[33] P. Bresson, J.-F. Bryche, M. Besbes, J. Moreau, P.-L. Karsenti, P. G. Charette, D. Morris, M. Canva, *Phys. Rev. B* **2020**, *102*, 155127.
[34] M. Y. Li, C. H. Chen, Y. Shi, L. J. Li, *Mater. Today* **2016**, *19*, 322.
[35] G. D. Nessim, M. Seita, K. P. O'Brien, A. J. Hart, R. K. Bonaparte, R. R. Mitchell, C. V. Thompson, *Nano Lett.* **2009**, *9*, 3398.
[36] A. Rahmani, H. Rahmani, A. Zonouzi, *Mater. Res. Express* **2017**, *4*, 125024.
[37] J. Liu, D. Xue, *Mater. Res. Bull.* **2010**, *45*, 309.
[38] K. Osakada, A. Taniguchi, E. Kubota, S. Dev, K. Tanaka, K. Kubota, T. Yamamoto, *Chem. Mater.* **1992**, *4*, 562.
[39] P. Kumar, M. Gusain, R. Nagarajan, *Inorg. Chem.* **2012**, *51*, 7945.
[40] S. Goel, F. Chen, W. Cai, *Small* **2014**, *10*, 631.
[41] A. Villa, A. M. Ross, R. Gotti, M. Lamperti, F. Scotognella, G. Cerullo, M. Marangoni, *OSA Continuum* **2021**, *4*, 2837.
[42] A.-L. Calendron, H. Çankaya, G. Cirmi, F. X. Kärtner, *Opt. Express* **2015**, *23*, 13866.
[43] D. Brida, C. Manzoni, G. Cerullo, *Opt. Lett.* **2012**, *37*, 3027.
[44] A. Oriana, J. Réhault, F. Preda, D. Polli, G. Cerullo, *J. Opt. Soc. Am. A* **2016**, *33*, 1415.
[45] J. Réhault, R. Borrego-Varillas, A. Oriana, C. Manzoni, C. P. Hauri, J. Helbing, G. Cerullo, *Opt. Express* **2017**, *25*, 4403.
[46] A. Perri, *J. Phys. B: At., Mol. Opt. Phys.* **2021**, *54*, 113001.